RA'EGA
O ESPAÇO GEOGRÁFICO EM ANÁLISE
https://revistas.ufpr.br/raega

ISSN eletrônico 2177-2738
RA'EGA, Curitiba, PR, V.62, n.1, p. 27–43, 4/2025
http://dx.doi.org/10.5380/raega.v62i1.98056

Analysis of biophysical parameters (vegetation and land surface temperature) with satellite images using the Google Earth Engine platform

Análise de parâmetros biofísicos (vegetação e temperatura de superfície terrestre) com imagens de satélite utilizando a plataforma Google Earth Engine

Bruna Borges da Rocha*

*Centro de Pesquisa e Estudos Ambientais (CPEA), Universidade do Extremo Sul Catarinense, brunabrgeo@gmail.com

http://dx.doi.org/10.5380/raega.v62i1.98056

Abstract

Urbanization exerts ecological and climatic impacts, and one of which is the increase in Land Surface Temperature (LST) in urban environments. Remote sensing enables the acquisition of satellite data capable of providing historical and current information from various regions worldwide. In addition to LST information, the identification of photosynthetically active vegetation is achievable through the application of the Normalized Difference Vegetation Index (NDVI). This study investigated the patterns of land surface temperature and their relationship with the vegetation index in areas influenced by urbanization in the city of Joinville - SC, using the Normalized Difference Vegetation Index (NDVI) as a biophysical parameter of surface emissivity. The Google Earth Engine (GEE) platform was used for the main processes and calculations, enabling access to cloud-based datasets from the Landsat 8 collection. The LST was obtained through surface emissivity, extracted via NDVI. The results indicate higher LST values in impermeable environments, with little or no vegetation. Thus, the research demonstrated that higher LST values result from the influence of lower NDVI values, highlighting the relevance of green areas in built environments.

Keywords:
Remote sensing, Urbanization, Landsat 8.

Resumo

O fenômeno da urbanização causa impactos ecológicos e climáticos, e um desses impactos é o aumento da Temperatura de Superfície Terrestre (TST) em ambientes urbanos. Por meio do sensoriamento remoto é possível obter dados de satélites capazes de fornecer informações históricas e atuais de diversas regiões no mundo. Além de informações sobre TST, também é possível identificar áreas com presença de vegetação fotossinteticamente ativa aplicando-se o Índice de

ISSN eletrônico 2177-2738
RA'EGA, Curitiba, PR, V.62, n.1, p. 27–43, 4/2025
http://dx.doi.org/10.5380/raega.v62i1.98056

Vegetação por Diferença Normalizada (IVDN). Este estudo objetivou analisar os padrões de temperatura de superfície terrestre e a sua relação com o índice de vegetação em áreas influenciadas pela urbanização no município de Joinville - SC, utilizando como parâmetro biofísico de emissividade de superfície o Índice de Vegetação por Diferença Normalizada (IVDN). A plataforma Google Earth Engine (GEE) é utilizada para os principais processos e cálculos, permitindo a obtenção de conjuntos de dados disponíveis em nuvem a partir da coleção Landsat 8. A TST foi obtida através da emissividade de superfície, extraída por meio do IVDN. Os resultados indicam valores maiores de TST em ambientes impermeáveis, com pouca ou nenhuma vegetação. Com isso, a pesquisa mostrou que valores maiores de TST decorrem da influência de valores menores de IVDN, ressaltando a relevância de áreas verdes em ambientes construídos.
Palavras-chave:
Sensoriamento remoto, Urbanização, Landsat 8.

I. INTRODUCTION

Concerns about rising air temperatures in urban environments have prompted intensive research efforts to better understanding this phenomenon (Avdan; Jovanovska, 2016; Espinoza-Molina et al., 2022; Tesfamariam; Govindu; Uncha, 2023). Through remote sensing, researchers can utilize digital processing of satellite imagery to monitor environmental and climatic changes (Baloloy et al., 2019).

Among the most widely utilized satellites is Landsat 8, which provides a historical archive of images beginning in 2013, the year it was launched by the National Aeronautics and Space Administration (NASA), as noted by the U.S. Geological Survey (USGS) (USGS, 2023). Images captured by Landsat 8, along with its sensors—the Operational Land Imager (OLI) and the Thermal Infrared Sensor (TIRS)—enable the generation of numerous geospatial datasets, including Land Surface Temperature (LST) measurements derived from its thermal bands (Lima et al., 2023).

Investigations into LST are critical for assessing urbanization impacts, such as the reduction of forested areas (Medeiros et al., 2023), which disrupt the natural resources essential for human survival. One effective method for identifying vegetated areas involves the application of the Normalized Difference Vegetation Index (NDVI) (Rouse et al., 1974; Alcantara et al., 2019; Zhao et al., 2022). NDVI facilitates the analysis of land use and land cover while providing insight into the health and vigor of vegetation (Liguori; Monteiro, 2023).

The absence of vegetation on the ground increases the incidence of surface radiation, particularly in built-up areas where soil impermeability restricts evapotranspiration, resulting in higher Land Surface Temperature (LST) values (Wang et al., 2022). Consequently, identifying the relationship between environmental variables in regional studies can provide detailed insights into specific environments.

ISSN eletrônico 2177-2738
RA'EGA, Curitiba, PR, V.62, n.1, p. 27–43, 4/2025
http://dx.doi.org/10.5380/raega.v62i1.98056

The Google Earth Engine (GEE) platform is commonly used for acquiring and processing large volumes of images and applying algorithms. It offers a wide range of geospatial datasets and enables cloud-based processing, facilitating rapid and large-scale analyses (Alcantara et al., 2019; Chakraborty et al., 2021; Označillová et al., 2022; Yang et al., 2022).

Within this context, the study aims to analyze patterns of land surface temperature and their relationship with the vegetation index in areas influenced by urbanization in the municipality of Joinville, SC. The Normalized Difference Vegetation Index (NDVI) is employed as a biophysical proxy of surface emissivity, utilizing the Google Earth Engine (GEE) platform. GEE provides publicly available images and supports a variety of applications, enabling researchers to conduct more robust and dynamic analyses through programming languages.

For this study, using the GEE platform, images with the lowest percentage of cloud cover were filtered, ensuring consistency by selecting the same seasonal period. From the selected high-quality images, key products were generated to estimate Land Surface Temperature (LST). NDVI is one such product, used to derive proportion of vegetation and surface emissivity. Initially, the images were reprojected and cropped to the desired area, generating the top-of-atmosphere radiance and brightness temperature products, with LST serving as the final output. Statistical analyses were then conducted using the LST and NDVI data to produce insights for the case study. Comparing data from different dates further reinforces the results, ensuring consistency and enabling the identification of modification patterns.

As Gao et al. (2021) suggest, considering contemporary dynamics and increasing human impacts, it is essential to find solutions to environmental issues and foster the development of more sustainable cities. In this context, the research contributes to both science and society by elucidating the relationship between key variables associated with urbanization impacts and deforestation.

II. Material and Methods

The following sections provide a detailed description of information relevant to the municipality of Joinville, the processes undertaken to generate the necessary research outputs, and complementary data used in the analyses.

Studied area

The study area corresponds to the municipality of Joinville, located in the northern mesoregion of the state of Santa Catarina, Brazil. It spans a total area of 1.128 km² and, according to the Digital Elevation Model

ISSN eletrônico 2177-2738
RA'EGA, Curitiba, PR, V.62, n.1, p. 27–43, 4/2025
http://dx.doi.org/10.5380/raega.v62i1.98056

(DEM) derived from the *Shuttle Radar Topography Mission* (SRTM), has an approximate altitude of up to 1.312 meters (Figure 1). Joinville is the most populous city in the state, with a population of 616,317 inhabitants, according to the latest census conducted by the Brazilian Institute of Geography and Statistics (IBGE, 2022).

The municipality is in the Atlantic Forest Biome, with Dense Ombrophilous Forest as its most representative vegetation type. This forest is characterized by various successional stages and is renowned for its abundance and richness of species (Mantovani et al., 2005).

According to the Köppen climate classification, the region has a Cfa climate, described as humid subtropical with no dry season, hot summers, monthly temperatures ≥22°C in the warmest month, and between ≥-3°C and <18°C in the coldest month, with monthly precipitation exceeding 40 mm (Alvares et al., 2013). The Cfb climate is also present in the region, characterized by temperatures below 22°C and at least four months with temperatures above 10°C (Alvares et al., 2013).

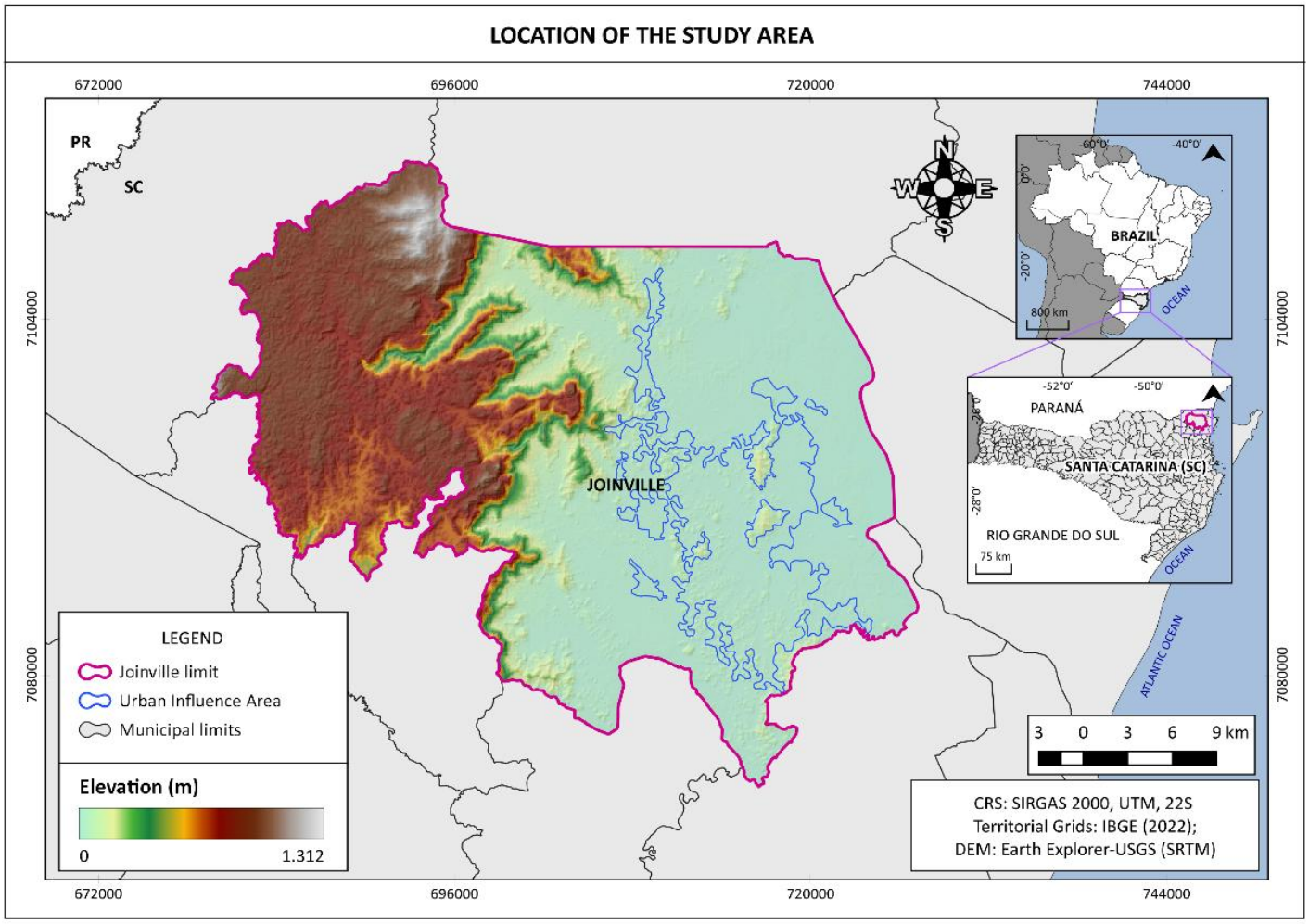

Figure 1 – Location of Joinville, State of Santa Catarina, Brazil.

Data Collection

ISSN eletrônico 2177-2738
RA'EGA, Curitiba, PR, V.62, n.1, p. 27–43, 4/2025
http://dx.doi.org/10.5380/raega.v62i1.98056

For data production, Landsat 8 satellite images (LANDSAT/LC08/C02/T1) available on the Google Earth Engine (GEE) platform were used. The images were acquired for the years 2014 and 2023 during the same seasonal period (winter). High-quality images were selected based on the lowest percentage of cloud cover, cropped, and reprojected to the appropriate coordinate system for the study area. All variable calculations were performed on the GEE platform using the JavaScript programming language. Details about the Landsat 8 satellite and the metadata for the images are provided in Table 1.

Table 1 – Landsat 8 satellite data and images used in GEE

Satellite Data

Satellite	Band	Sensor	Spatial Resolution	Spectral Resolution (μm)	Activity Period
Landsat 8	B10	TIRS	100m➡30m	10.6 – 11.2	11-02-2013 - present
	B4	OLI	30m	0.630 – 0.680	
	B5	OLI	30m	0.845 – 0.885	

Imagem Data

Image ID	Date	Cloud Cover (%)	Orbit
LANDSAT/LC08/C02/T1/LC08_220078_20230803	03-08-2023	1.52	78
LANDSAT/LC08/C02/T1/LC08_220078_20140826	26-08-2014	18.05	

Notes: Band 10 (B10) data were resampled to 30m to match the spatial resolution of the OLI sensor's multispectral bands. The best available images still contained some cloud cover; however, the study area was not affected. Source: USGS (2023). Author: Bruna Borges da Rocha.

For the following equations, the reference bases used were: Van de Griend and Owe (1993); Avdan and Jovanovska (2016); Baloloy et al. (2019); Jeevalakshmi, Reddy and Manikiam (2019); Fashae et al. (2020); Roy et al. (2021); Roy and Bari (2022); Castro et al. (2023); Tesfamariam, Govindu and Uncha (2023); Zaloti et al. (2023).

Determination of radiance and brightness temperature

For these steps, the thermal band (B10) from the *Thermal Infrared Sensor* (TIRS) was selected. The gray-level values were converted to *Top of Atmosphere* (TOA) radiance (Lλ), and from this information, the *Brightness Temperature* (BT) was calculated.

The parameters used are provided in the metadata of the thermal band. On the GEE platform, the process was carried out using the "ee . Algorithms . Landsat . calibratedRadiance" algorithm available on the Google Developers page, as shown in the following equation:

ISSN eletrônico 2177-2738
RA'EGA, Curitiba, PR, V.62, n.1, p. 27–43, 4/2025
http://dx.doi.org/10.5380/raega.v62i1.98056

$$L_\lambda = M_L * Qcal + A_L \quad (1)$$

Where:

L_λ = spectral radiance in Watts / (m^2 * sr * µm).

M_L = multiplicative rescaling factor (RADIANCE_MULT_BAND_10).

Qcal = quantized calibrated pixel value in digital number (Band 10).

A_L = additive rescaling factor (RADIANCE_ADD_BAND_10).

The Brightness Temperature (BT) in Kelvin was obtained using the values of the constants K1 and K2, which are also provided in the image metadata, as shown in the following equation:

$$BT = \frac{K_2}{ln\left(\frac{K_1}{L\lambda}+1\right)} \quad (2)$$

Where:

K1 = calibration constant 1 = 774.89 (K1_CONSTANT_BAND_10).

K2 = calibration constant 2 = 1321.08 (K2_CONSTANT_BAND_10).

ln = natural logarithm.

Determination of vegetation index, emissivity, and land surface temperature

For these steps, the vegetation index was calculated by first selecting the red (B4) and near-infrared (B5) bands from the *Operational Land Imager* (OLI) sensor. Subsequently, the proportion of vegetation (Pv) was computed. The Normalized Difference Vegetation Index (NDVI), initially proposed by Rouse et al. (1974), was derived using the red (B4) and near-infrared (B5) bands, as shown in the following equation:

$$NDVI = \frac{B5-B4}{B5+B4} \quad (3)$$

The calculation of the proportion of vegetation (Pv) was necessary for the subsequent processes, following the equation:

ISSN eletrônico 2177-2738
RA'EGA, Curitiba, PR, V.62, n.1, p. 27–43, 4/2025
http://dx.doi.org/10.5380/raega.v62i1.98056

$$Pv = \left(\frac{NDVI - NDVI\ min}{NDVI\ max - NDVI\ min}\right)^2 \quad (4)$$

Where:

min. = minimum.

max = maximum.

With the proportion of vegetation calculated, the surface emissivity (ε) was then obtained:

$$eissivity\ (\varepsilon) = 0.004 * P_v + 0.986 \quad (5)$$

Using the emissivity results, the Land Surface Temperature (LST) was determined. However, it was necessary to subtract 273.15 to convert the result from Kelvin to degrees Celsius (°C), since the result was originally in Kelvin. Below is the equation used to calculate LST.

$$LST = \frac{BT}{\{1+\left[\frac{\lambda BT}{\rho}\right].ln\ \varepsilon\}} - 273.15 \quad (6)$$

Where:

ln = natural logarithm

λ = wavelength of emitted radiance (10.8).

ρ = 1.438×10^{-2} mK (14388).

ε = surface emissivity.

For the statistical analyses between LST and NDVI, point samples were collected within the urban influence boundary of the municipality, as provided by the Environmental Data and Information Database (BDIA) (IBGE, 2023). The samples were taken from locations identified in the images to extract pixel values. Additionally, within the urban influence boundary, pixel values from the entire LST and NDVI images were extracted to support the data analysis. These processes were conducted using the software QGIS 3.28, along with cartographic finalization. Statistical analyses were performed using the Python programming language via Jupyter Notebook.

Figure 2 illustrates the sequence of steps undertaken to develop and obtain the research results.

ISSN eletrônico 2177-2738
RA'EGA, Curitiba, PR, V.62, n.1, p. 27–43, 4/2025
http://dx.doi.org/10.5380/raega.v62i1.98056

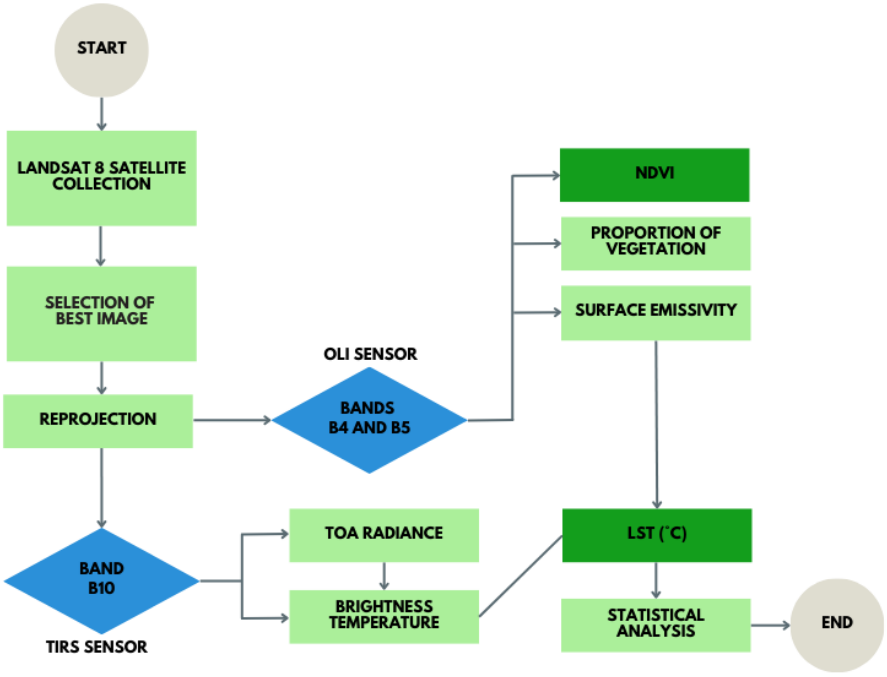

Figure 2 – Flowchart of the methodological steps.

To support the data analyses, GEE also provides regional statistical analysis through the reduction function, which allows the extraction of minimum and maximum LST values for a defined area by simply delimiting it. Additionally, graphs were created comparing built environments with forested areas within the urban influence boundary, as well as the area in hectares for each temperature range in the images, considering the entire municipality.

All products generated on the GEE platform are available through the link provided in Box 1.

Box 1 – Access to the products generated on the Google Earth Engine platform.

Data Type	Access link
General Data	https://code.earthengine.google.com/5df1bfd87cbea13788e0548becff33a0
Radiance and Brightness Temperature	https://code.earthengine.google.com/cbce586444a25a29d5e49e936aaa6fff
Emissivity and NDVI	https://code.earthengine.google.com/eb3a3cdbce4dce9b8a48f78a049df28c
LST	https://code.earthengine.google.com/fcabcddc80966c7a7e3b040bdb6662ad

Notes: Box with link for direct access to data on the GEE platform. Source: GEE. Author: Bruna Borges da Rocha.

III. RESULTS AND DISCUSSION

The true-color compositions for each studied date can be viewed in Figure 3. The results are derived from the composition of the B4, B3, and B2 bands of the OLI sensor, representing the study area and the

ISSN eletrônico 2177-2738
RA'EGA, Curitiba, PR, V.62, n.1, p. 27–43, 4/2025
http://dx.doi.org/10.5380/raega.v62i1.98056

boundary of the municipality's urban influence zone, which accounts for approximately 144 km² (12.75%) of the municipality's total area.

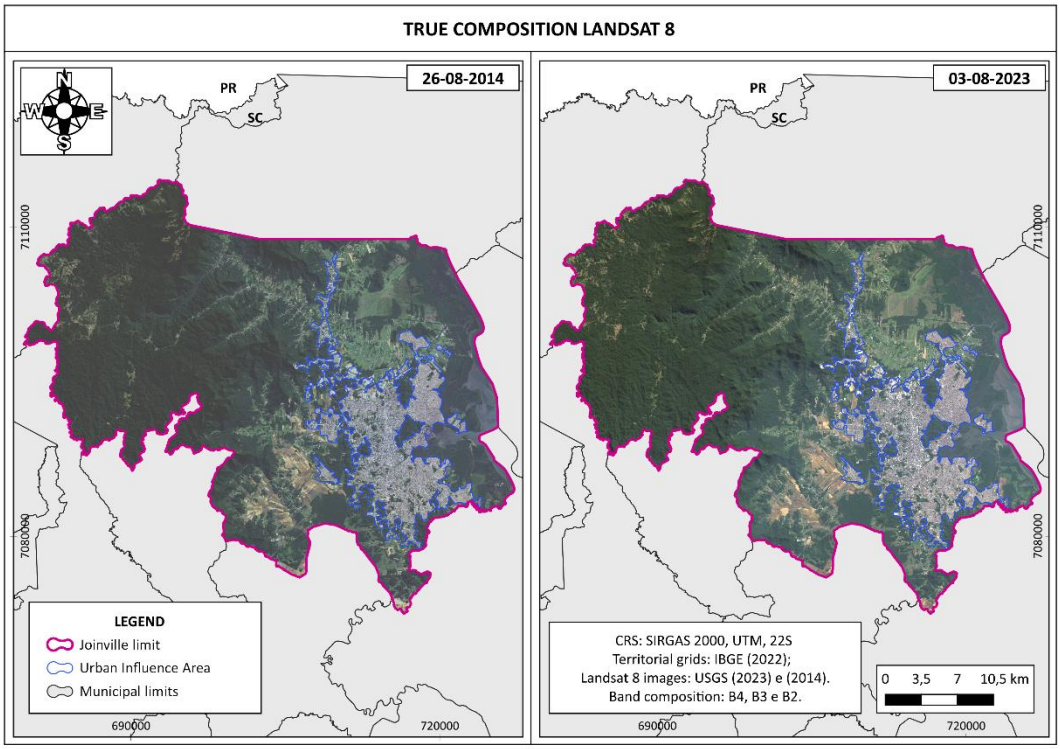

Figure 3 – True-color Landsat 8 composition for the municipality of Joinville and the urban influence boundary.

The results of the LST estimation can be observed in Figure 4. The classification of both images shows that the highest LST values are concentrated in the urban influence areas, with little or no vegetation. Temperatures in the 30°C to 35°C range cover approximately 2.118 hectares in 2014 and about 48.724 hectares in 2023. Temperatures between 25°C and 30°C are predominant in both images, corresponding to approximately 65.053 hectares in 2014 and 63.507 hectares in 2023. Temperatures ≤25°C account for approximately 45.619 hectares in the 2014 image, while in the 2023 image, these temperatures only represent 438 hectares. These results confirm the predominance of lower surface temperatures in the 2014 classification. Additionally, temperatures above 35°C are also observed, forming small heat islands, particularly in impermeable environments that are prevalent in urban areas.

ISSN eletrônico 2177-2738
RA'EGA, Curitiba, PR, V.62, n.1, p. 27–43, 4/2025
http://dx.doi.org/10.5380/raega.v62i1.98056

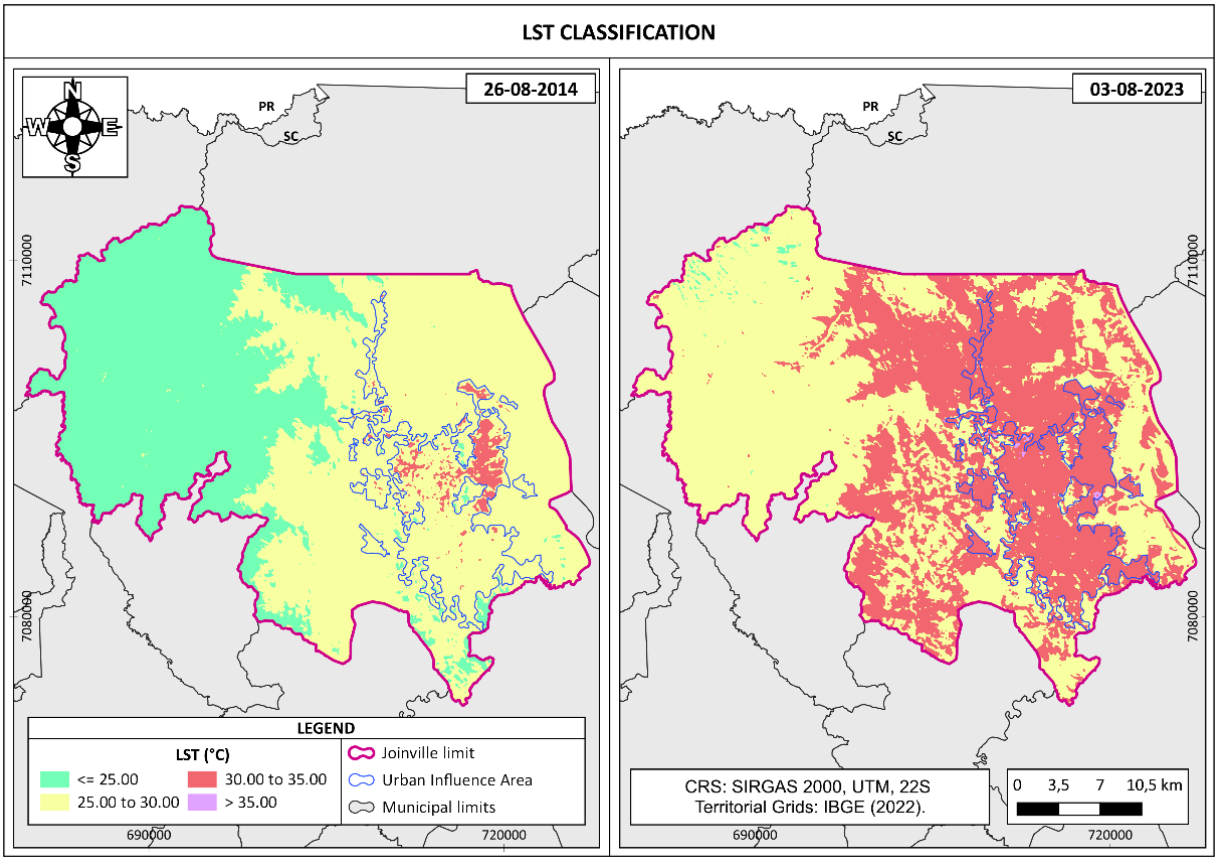

Figure 4 – Classification of LST estimation for the studied dates.

Figure 5 presents the histograms of LST value variation, and Figure 6 displays the histograms of NDVI value variation, considering all pixels within the urban influence boundary. Statistical analyses of the LST data revealed that, for 2014, the mean pixel value was 28,59°C, the median was 28,67°C, and the mode was 28,81°C. For 2023, the mean was 31,71°C, the median 31,81°C, and the mode 32,02°C. The analysis also indicated that the variance in the 2014 data was slightly higher (1,74) compared to 2023 (1,24). Regarding the standard deviation, 2014 showed a value of 1,32°C, while 2023 had a lower value of 1,11°C, indicating greater variability in LST for 2014 compared to 2023.

For NDVI, in 2014, the mean pixel value was 0,20, the median was 0,16, and the mode was 0,2. In 2023, the mean was 0,16, the median 0,13, and the mode 0.09. Statistical analysis also showed that the variance in the 2014 data was slightly higher (0,01) compared to 2023 (0,009). The standard deviation results indicated that NDVI in 2014 (0,11) exhibited greater variability than in 2023 (0,09). The higher pixel value variability in 2014 suggests that the LST and NDVI values were more dispersed around the mean compared to 2023.

ISSN eletrônico 2177-2738
RA'EGA, Curitiba, PR, V.62, n.1, p. 27–43, 4/2025
http://dx.doi.org/10.5380/raega.v62i1.98056

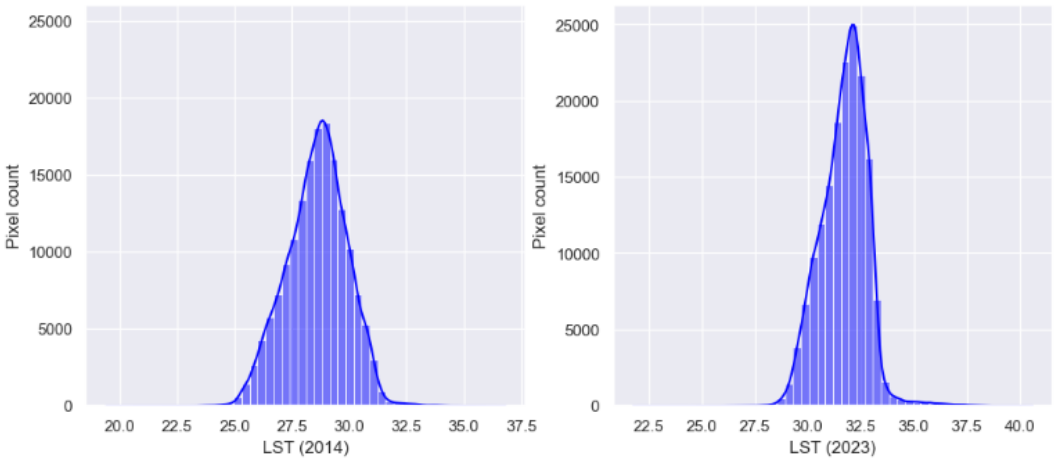

Figure 5 – LST variation within the urban influence boundary.

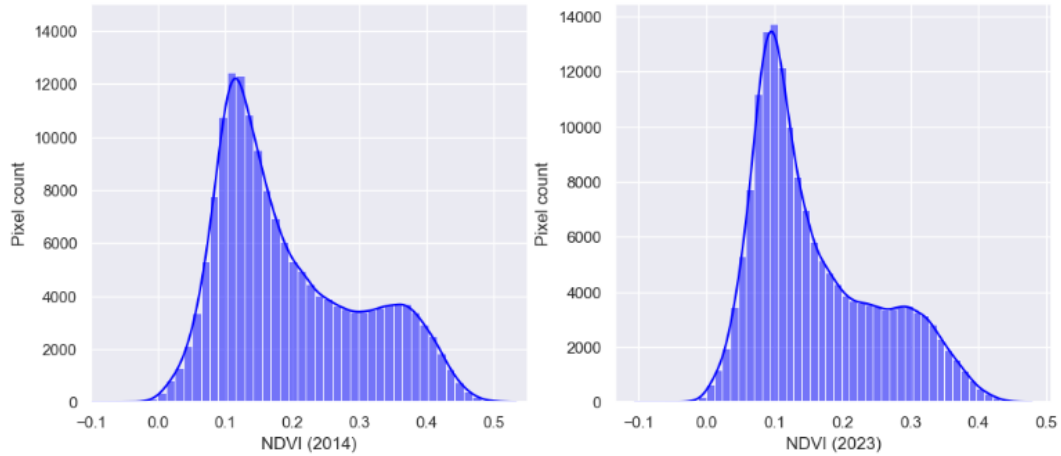

Figure 6 – NDVI variation within the urban influence boundary.

In Figure 7, these results reveal similar trends between the classifications for both dates, also highlighting the relationship between LST and NDVI variables. According to the classification, the lowest NDVI values (≤ 0,00 to 0,15) in terrestrial environments are concentrated in anthropized areas, many of which have been converted into impermeable surfaces.

ISSN eletrônico 2177-2738
RA'EGA, Curitiba, PR, V.62, n.1, p. 27–43, 4/2025
http://dx.doi.org/10.5380/raega.v62i1.98056

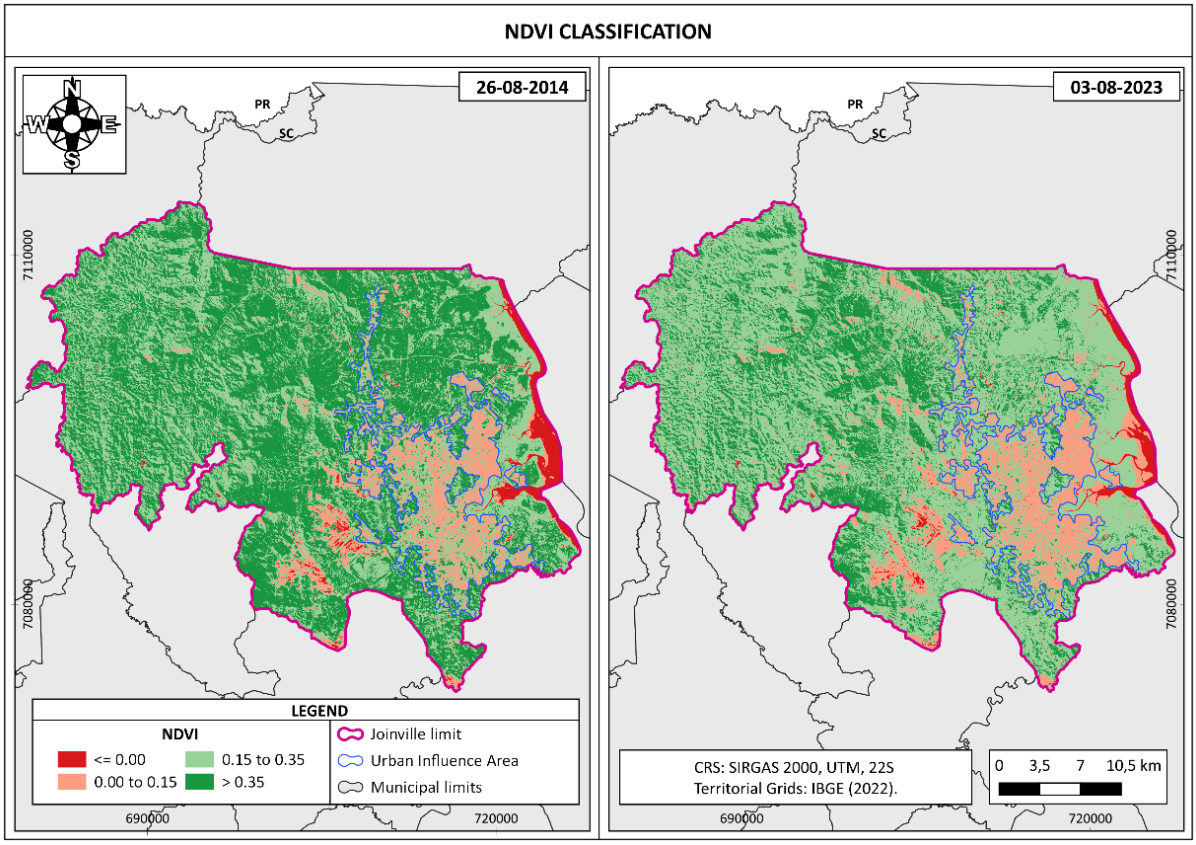

Figure 7 – NDVI classification for the years 2014 and 2023.

Regarding the statistical analyses derived from the samples within Joinville's urban influence area, the data are presented in Table 2 and the scatter plots in Figure 8. For both dates, the results are significant at the 5% level (T-Student) and indicate a moderate negative correlation between the variables (R). Linear regression (Y) also allowed for the estimation of LST (dependent variable) based on specified NDVI values (independent variable). According to the coefficient of determination (R^2), 38% of the LST data in the 2014 image can be explained by the NDVI variable, while in the 2023 image, 42% of the LST data can be explained by NDVI.

Table 2 – Statistical data LST x NDVI (sampling).

Date	R	T-Student	T critical	Y	R^2	Estimation
26-08-2014	-0,62	-20,67	1,96	a = 30,84 b = -9,36	0,38	if NDVI= 0,5 then LST=26,16
03-08-2023	-0,65	-22,75	1,96	a = 33,65 b = -10,02	0,42	if NDVI= 0,5 then LST=28,64

Notes: Statistical data between LST and NDVI considering sampling in the urban area of influence of the city of Joinville. Author: Bruna Borges da Rocha.

ISSN eletrônico 2177-2738
RA'EGA, Curitiba, PR, V.62, n.1, p. 27–43, 4/2025
http://dx.doi.org/10.5380/raega.v62i1.98056

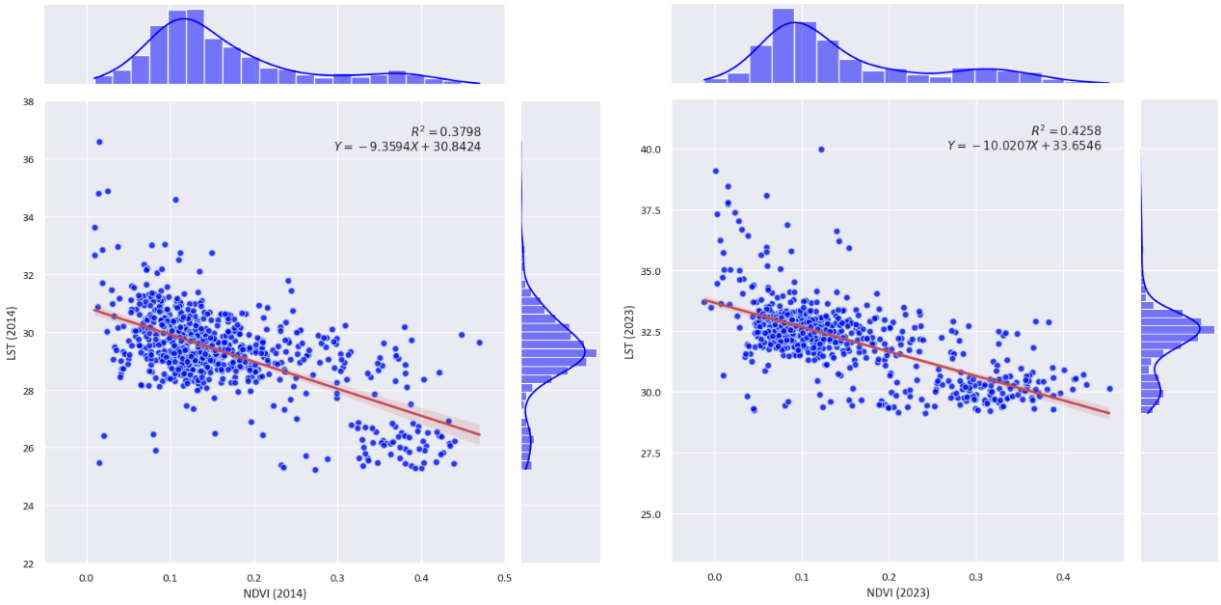

Figure 8 – Correlation with linear regression between NDVI and LST from samples within the urban influence boundary.

Apart from areas with water bodies, which have negative values, NDVI values in terrestrial environments close to -1 may indicate low photosynthetic activity or vegetation loss, whereas values closer to 1 suggest the opposite (Huang; Yang; Huang, 2021). Accordingly, the NDVI analysis identified areas with higher photosynthetic activity, resulting from greater vegetation cover, which can reduce the penetration of radiation to the Earth's surface (Espinoza-Molina et al., 2022).

LST values are lower in natural environments due to the presence and greater vigor of vegetation, a factor identified through NDVI (Fashae et al., 2020; Hao et al., 2019; Saleem et al., 2020; YU; Li, 2022; Lima et al., 2023; Zaloti et al., 2023). In urban environments, vegetation clusters or green areas help to mitigate surface temperatures (Saleem et al., 2020; Najafzadeh et al., 2021). NDVI values can also vary based on precipitation and soil moisture conditions (Huang; Yang; Huang, 2021; Lima et al., 2023; Sousa et al., 2023). Thus, various environmental variables can influence LST values.

In addition to built-up areas and exposed soil, regions covered by pastures and grasses can also exhibit higher LST values, as they tend to retain surface water, potentially impacting groundwater recharge and disrupting evapotranspiration dynamics (Jardim et al., 2022). When evapotranspiration rates are low, the latent heat flux decreases, thereby hindering surface cooling (Nill et al., 2019; Espinoza-Molina et al., 2022). The findings of this study are further supported by Wang et al. (2022), who compared LST variations across different land use and cover classes and confirmed higher temperatures in impermeable, pasture, and agricultural areas.

ISSN eletrônico 2177-2738
RA'EGA, Curitiba, PR, V.62, n.1, p. 27–43, 4/2025
http://dx.doi.org/10.5380/raega.v62i1.98056

IV. CONCLUSION

The digital processing of satellite images through remote sensing using Landsat 8 imagery enabled the extraction of LST data via emissivity derived from NDVI across different dates, yielding satisfactory results. This effective method, widely utilized by numerous researchers, made it possible to identify areas with higher and lower LST values, as well as those with higher photosynthetic activity or denser vegetation cover through NDVI. A clear relationship was observed between increasing LST and decreasing NDVI, a trend corroborated by analyses within the urban influence boundary of the municipality of Joinville. Statistical analyses of these relationships confirmed the correlation between the variables and contributed to explaining part of the variability in LST values. Furthermore, comparing these results with previous studies revealed similar patterns, reinforcing their consistency and relevance. This external validation strengthens the reliability of the results, adding a critical dimension to the interpretation and applicability of the acquired data.

The research provides a broader and more accessible understanding of data acquisition and manipulation using the Google Earth Engine (GEE) platform. The platform proved crucial for the analytical processes, enabling efficient access to cloud-stored datasets while simultaneously contributing to a significant reduction in the volume of processed data. This technical aspect not only simplifies the execution of analyses but also represents an innovative approach to managing and utilizing large geospatial datasets.

The strategic importance of green areas is underscored in this context, as they mitigate thermal effects and reduce urban heat islands, highlighting the need to integrate natural elements into sustainable urban planning. Their relevance not only emphasizes the environmental dimension but also demonstrates the potential benefits of these strategies in improving quality of life and fostering more balanced and healthy urban environments. This duality of practical and conceptual contributions strengthens the impact and applicability of the research findings.

The primary limitation identified in the study lies in the fact that, beyond the influence of vegetation, adjacent variables such as elevation variation and precipitation may also affect surface temperature. Thus, a more comprehensive understanding of the LST phenomenon requires detailed and multivariate analyses. This multifactorial complexity represents the main intrinsic limitation of the study, emphasizing the need for further investigations to capture all the nuances involved in the area's thermal dynamics.

Future research could focus on expanding and refining the data by incorporating additional climatic variables for a more comprehensive analysis. Furthermore, specific studies on the impact of different types of

ISSN eletrônico 2177-2738
RA'EGA, Curitiba, PR, V.62, n.1, p. 27–43, 4/2025
http://dx.doi.org/10.5380/raega.v62i1.98056

urban vegetation cover and their effect on local temperatures may provide valuable indicators for sustainable urban planning strategies. A deeper exploration of GEE's capabilities could also pave the way for more advanced and extensive analyses, contributing to the ongoing advancement of understanding thermal phenomena in urban environments.

V. REFERENCES

ALCANTARA, C. A.; ESCOTO, J. D.; BLANCO, A. C.; BALOLOY, A. B.; SANTOS, J. A. Geospatial assessment and modeling of urban heat islands in Quezon City, Philippines using OLS and geographically weighted regression. The International Archives of the Photogrammetry, Remote Sensing and Spatial Information Sciences, v. 42, p. 85-92, 2019.

ALVARES, C. A.; STAPE, J. L.; SENTELHAS, P. C.; MORAES, G.; SPAROVEK, G. Köppen's Climate Classification Map for Brazil. Meteorologische Zeitschrift, v. 22, n. 6, p. 711-728, 2013.

AVDAN, U.; JOVANOVSKA, G. Algorithm for automated mapping of land surface temperature using LANDSAT 8 satellite data. Journal of sensors, v. 2016, n. 1, p. 1480307, 2016.

BALOLOY, A.; CRUZ, J. A.; BLANCO, A. C.; LUBRICA, N. V.; VALDEZ, C. J.; CAJUCOM, E. P. Spatiotemporal multi-satellite biophysical data analysis of the effect of urbanization on land surface and air temperature in Baguio City, Philippines. The International Archives of the Photogrammetry, Remote Sensing and Spatial Information Sciences, v. 42, p. 47-54, 2019.

CASTRO, N. A. V.; ALMADRONES-REYES, K. J.; LIMBO-DIZON, J. E.; REDEÑA-SANTOS, J. C.; DAGAMAC, N. H. Applying geomatic analyses using Landsat imagery in Occidental Mindoro, the Philippines. 2023.

CHAKRABORTY, T. C.; LEE, X.; ERMIDA, S.; ZHAN, W. On the land emissivity assumption and Landsat-derived surface urban heat islands: A global analysis. Remote Sensing of Environment, v. 265, p. 112682, 2021.

ESPINOZA-MOLINA, J.; ACOSTA-CAIPA, K.; CHAMBE-VEGA, E.; HUAYNA, G.; PINO-VARGAS, E.; ABAD, J. Spatiotemporal analysis of urban heat islands in relation to urban development, in the vicinity of the Atacama Desert. Climate, v. 10, n. 87, 2022. DOI: https://doi.org/10.3390/cli10060087.

FASHAE, O. A.; LAWAL, O.; IGE-ETTI, M.; AGBATOYE, O. Land use/land cover change and land surface temperature of Ibadan and environs, Nigeria. Environmental Monitoring and Assessment, v. 192, p. 1-18, 2020.

GAO, W.; ZHANG, S.; RAO, X.; LIN, X.; LI, R. Landsat TM/OLI-based ecological and environmental quality survey of the Yellow River Basin, Inner Mongolia Section. Remote Sensing, v. 13, n. 21, p. 4477, 2021.

HAO, B.; ZHANG, Q.; WANG, X.; LIU, S.; YANG, D.; LIU, Z. Land use change and climate variation in the Three Gorges Reservoir catchment from 2000 to 2015 based on the Google Earth Engine. Sensors, v. 19, n. 9, p. 2118, 2019.

HUANG, C.; YANG, Q.; HUANG, W. Analysis of the spatial and temporal changes of NDVI and its driving factors in the Wei and Jing River Basins. International Journal of Environmental Research and Public Health, v. 18, n. 22, p. 11863, 2021.

IBGE - Instituto Brasileiro de Geografia e Estatística. BDiA - Banco de Informações Ambientais | BDiA - web. Vegetação. 2023. Disponível em: https://bdiaweb.ibge.gov.br/#/consulta/vegetacao. Acesso em 11 out. 2023.

ISSN eletrônico 2177-2738
RA'EGA, Curitiba, PR, V.62, n.1, p. 27–43, 4/2025
http://dx.doi.org/10.5380/raega.v62i1.98056

IBGE - Instituto Brasileiro de Geografia e Estatística. Cidades. População. 2022. Disponível em: https://cidades.ibge.gov.br/brasil/sc/joinville/panorama. Acesso em 11 Out. 2023.

JARDIM, A. M. R. F.; MORAIS, J. E. F.; SOUZA, L. S. B.; SILVA, T. G. F. Understanding interactive processes: a review of CO2 flux, evapotranspiration, and energy partitioning under stressful conditions in dry forest and agricultural environments. Environmental Monitoring and Assessment, v. 194, n. 10, p. 677, 2022.

JEEVALAKSHMI, D.; REDDY, S. N.; MANIKIAM, B. Estimation of land surface temperature over vegetated region using AVHRR sensor data and validation with in-situ measurements. International Journal of Modern Electronics and Communication Engineering (IJMECE), v. 7, n. 2, p. 199–204, mar. 2019.

LIGUORI, I. N.; MONTEIRO, L. M. Avaliação comparativa da temperatura de superfície e indicadores geoespaciais na cidade de São Paulo. Encontro Nacional de Conforto no Ambiente Construído, v. 17, p. 1-10, 2023.

LIMA, T. P.; FRANÇA, L. C. J.; FERRAZ, F. T.; SILVA, J. B. L.; FERREIRA, M. E.; SILVA, A. R.; SILVA, D. P. Correlação entre as transformações da cobertura e uso da terra com variáveis climáticas e ambientais na região do Matopiba, Brasil. Revista do Departamento de Geografia, v. 43, p. e202077-e202077, 2023.

MANTOVANI, M.; JUNQUEIRA, A. G.; MARTINS, F. R.; SANTOS, F. A. Diversity of species and successional structure of a secondary formation in an Atlantic rain forest. 2005.

MEDEIROS, M.; PATRIOTA, E.; SILVA, L.; COELHO, V. A relação entre ilhas de calor urbana superficial, ocupação do solo e conforto térmico: um estudo da cidade de João Pessoa, Brasil. Encontro Nacional de Conforto no Ambiente Construído, v. 17, p. 1-10, 2023.

NAJAFZADEH, F.; MOHAMMADZADEH, A.; GHORBANIAN, A.; JAMALI, S. Spatial and temporal analysis of surface urban heat island and thermal comfort using Landsat satellite images between 1989 and 2019: A case study in Tehran. Remote Sensing, v. 13, n. 21, p. 4469, 2021.

NILL, L.; ULLMANN, T.; KNEISEL, C.; SOBIECH-WOLF, J.; BAUMHAUER, R. Assessing spatiotemporal variations of Landsat land surface temperature and multispectral indices in the Arctic Mackenzie Delta Region between 1985 and 2018. Remote Sensing, v. 11, n. 19, p. 2329, 2019.

ONAČILLOVÁ, K.; GALLAY, M.; PALUBA, D.; PÉLIOVÁ, A.; TOKARČÍK, O.; LAUBERTOVÁ, D. Combining Landsat 8 and Sentinel-2 data in Google Earth Engine to derive higher resolution land surface temperature maps in urban environment. Remote Sensing, v. 14, n. 16, p. 4076, 2022.

ROUSE, J. W.; HAAS, R. H.; SCHELL, J. A.; DEERING, D. W. Monitoring vegetation systems in the Great Plains with ERTS. NASA Spec. Publ., v. 351, n. 1, p. 309, 1974.

ROY, B.; BARI, E. Examining the relationship between land surface temperature and landscape features using spectral indices with Google Earth Engine. Heliyon, v. 8, n. 9, 2022.

ROY, B.; BARI, E.; NIPA, N. J.; ANI, S. A. Comparison of temporal changes in urban settlements and land surface temperature in Rangpur and Gazipur Sadar, Bangladesh after the establishment of city corporation. Remote Sensing Applications: Society and Environment, v. 23, p. 100587, 2021.

SALEEM, M. S.; AHMAD, S. R.; REHMAN; S. U.; JAVED, M. A. Impact assessment of urban development patterns on land surface temperature by using remote sensing techniques: A case study of Lahore, Faisalabad and Multan district. Environmental Science and Pollution Research, v. 27, n. 32, p. 39865-39878, 2020.

SOUSA, J. H. S.; RIBEIRO, G. N.; FRANCISCO, P. R. M.; JÚNIOR, O. A.; SILVA, L. H. G. T.; NÓBREGA, J. L. Índices biofísicos da bacia hidrográfica do rio Sucuru-PB utilizando o Google Earth Engine. Revista Geama, v. 9, n. 3, p.

ISSN eletrônico 2177-2738
RA'EGA, Curitiba, PR, V.62, n.1, p. 27–43, 4/2025
http://dx.doi.org/10.5380/raega.v62i1.98056

86-94, 2023.

TESFAMARIAM, S.; GOVINDU, V.; UNCHA, A. Spatio-temporal analysis of urban heat island (UHI) and its effect on urban ecology: The case of Mekelle city, Northern Ethiopia. Heliyon, v. 9, n. 2, 2023.

USGS - U.S. Geological Survey. Landsat 8. 2023.Disponível em: https://www.usgs.gov/landsat-missions/landsat-8. Acesso em 11 Out. 2023.

VAN DE GRIEND, A. A.; OWE, M. On the relationship between thermal emissivity and the normalized difference vegetation index for natural surfaces. International Journal of Remote Sensing, v. 14, n. 6, p. 1119-1131, 1993.

WANG, A.; ZHANG, M.; KAFY, A. A.; TONG, B.; HAO, D.; FENG, Y. Predicting the impacts of urban land change on LST and carbon storage using InVEST, CA-ANN and WOA-LSTM models in Guangzhou, China. Earth Science Informatics, v. 16, n. 1, p. 437-454, 2022.

YANG, Z.; TIAN, J.; SU, W.; WU, J.; LIU, J.; LIU, W.; GUO, R. Analysis of ecological environmental quality change in the Yellow River Basin using the remote-sensing-based ecological index. Sustainability, v. 14, n. 17, p. 10726, 2022.

YU, H.; LI, L. Inferring land conditions in the Tumen River Basin by trend analysis based on satellite imagery and geoinformation. Sustainability, v. 14, n. 9, p. 5687, 2022.

ZALOTI, F. A.; SANTOS, P. S.; CARDOSO, D. M. C. Comparação entre a cobertura vegetal e a temperatura de superfície terrestre, em Lauro de Freitas na Bahia. Revista Brasileira de Sensoriamento Remoto, v. 4, n. 2, 2023.

ZHAO, X.; WANG, P.; YASIR, M.; LIU, Z. Decision support system based on spatial and temporal pattern evolution of ecological environmental quality in the Yellow River Delta from 2000 to 2020. Soft Computing, v. 26, n. 20, p. 11033-11044, 2022.